Ann. Geophys. Discuss., https://doi.org/10.5194/angeo-2019-34
Manuscript under review for journal Ann. Geophys.
Discussion started: 8 March 2019

Annales Geophysicae Discussions
Open Access
EGU

Long-term trends in the ionospheric response to solar EUV variations

Rajesh Vaishnav[1], Christoph Jacobi[1], and Jens Berdermann[2]

[1]Leipzig Institute for Meteorology, Universität Leipzig, Stephanstr. 3, 04103 Leipzig, Germany
[2]German Aerospace Center, Kalkhorstweg 53, 17235 Neustrelitz, Germany

Correspondence to: Rajesh Vaishnav (rajesh_ishwardas.vaishnav@uni-leipzig.de)

Abstract. The thermosphere-ionosphere system shows high complexity due to interaction with the continuously varying solar radiation flux. We investigate the ionospheric response to the temporal and spatial dynamics of the solar activity using 18 years (1999-2017) of total electron content (TEC) maps provided by the international GNSS service (IGS) and twelve solar proxies (F10.7, F1.8, F3.2, F8, F15, F30, He-II, MG-II index, Ly-α, Ca K, DSA and SSN). Cross-wavelet and Lomb Scargle periodogram (LSP) analysis are used to evaluate the different solar proxies in respect to their impact on the global mean TEC (GTEC), which is important for improved ionosphere modelling and forecasts. A 16-32 days period in all the solar proxies and GTEC has been identified. The maximum correlation at this time scale is observed between the He-II, Mg-II, and F30 with respect to GTEC, with an effective time delay of about one day. LSP analysis shows that the most dominant period is 27 days, which is based on mean solar rotation, followed by a 44-day periodicity. In addition, a semi-annual and an annual variation has been observed in GTEC, with the strongest correlation near the equator region where a time delay about 1-2 days exists. The wavelet variance estimation method is used to find the variance in the maximum of the solar cycles (SC) 23 (2000-2002) and 24 (2012-2014), for GTEC and F10.7 index, respectively. Wavelet variance estimation suggests that GTEC variance is highest for the seasonal timescale followed by the 16-32 days period, similar to the F10.7 index highest variance for the 16-32 days period. Variance during SC 23 is larger than during SC 24. The most suitable proxy to represent the solar activity at the time scales of 16-32 days and 32-64 days is He-II. The MG-II index, Ly-α, and F30 may be placed at the second as these indices show the strongest correlation with GTEC, but there are some differences between solar maximum and minimum. The F1.8 and DSA are of limited use to represent the solar impact on GTEC. Empirical orthogonal function (EOF) analysis of the TEC data shows that the first EOF components capture more than 86% of the variance, and the first three EOF components explain 99% of the total variance. EOF analysis suggests that the first component is associated with the solar flux.

1 Introduction

The interaction of solar radiation with the ionosphere is complicated due to several mechanisms with the potential to modulate the thermosphere-ionosphere (T-I) system at different timescales ranging from the 11-year solar cycle down to minutes (Chen et al., 2012). The ionosphere plasma response to solar EUV and UV variations has been widely studied using ground- and space-based observations (e.g. Schmölter et al., 2018), as

well as numerical and empirical modelling (e.g. Ren et al., 2018, Vaishnav et al., 2018a,b). These studies have shown, that the response of the ionosphere to solar EUV radiation variations takes 1-2 days for solar radiation changes within 27 days solar rotation period (e.g. Jakowski et al., 1991; Afraimovich et al., 2008; Min et al., 2009; Lee et al., 2012; Jacobi et al., 2016).

To understand the underlying mechanisms of the delay observed in ionospheric plasma, Jakowski et al. (1991) used a one-dimensional (1-D) numerical model to explain the ionospheric delay of about 1-2 days. They concluded that the ionospheric delay could be attributed to the delayed atomic oxygen density variation at 180 km height produced via O_2 photdissociation. Ren et al. (2018) performed multiple numerical experiments using the TIE-GCM model to investigate potential physical mechanisms which might be responsible for the ionospheric delay. Their simulation results revealed that photochemical, dynamic, and electrodynamic processes, as well as the geomagnetic activity, can be associated with the ionosphere response time. Vaishnav et al. (2018a) performed CTIPe model simulations to explore the dominant mechanisms and suggested that transport might be the leading process responsible for the ionospheric delay.

The T-I system is also influenced by different external forces, which include lower atmosphere forcing, geomagnetic as well as solar wind conditions. In the case of solar events, the forcing from above might even result in strong disturbances affecting the ionospheric delay. As a result, the ionospheric plasma behaviour is varying during different solar activity conditions.

The mean solar rotation period is approximately 27 days, and therefore similar periodic variations are expected in the ionospheric parameters, such as total electron content (TEC, measured in TECU: 1 TEC Unit = 10^{16} electrons/m^2), NmF2, etc. (e.g. Min et al., 2009). Hocke (2008) studied oscillations in the global mean TEC (GTEC) and solar EUV (MG-II index) at different time scales. He reported that oscillations observed in GTEC could be related to the ionising radiation changes.

Many studies have concentrated on the 27 days variations in ionospheric TEC against different solar EUV representatives. In order to understand the variability of the T-I system, the understanding of solar EUV variations is essential. Since direct EUV measurements before the space age were not available due to atmospheric absorption and are still not available in the full spectrum, solar proxies are frequently used to represent solar variability till today. The most widely used proxies for ionospheric applications are the F10.7 index (Maruyama, 2010), the MG-II index, and indices based on direct EUV measurements (e.g., Unglaub et al., 2011) like the Solar EUV Experiment (SEE) onboard the Thermosphere Ionosphere Mesosphere Energetics and Dynamics (TIMED) satellite (Woods et al., 2000). Using the latter poses the potential problem of satellite degradation (BenMoussa et al., 2013, Schmidtke et al., 2015), which may be overcome by repeated calibration or in-flight calibration as had been applied during the SolACES experiment on board the ISS (Schmidtke et al., 2014, 2015).

This paper investigates and evaluates the correlation between GTEC and different solar EUV proxies in the time period January 1999 till December 2017. The purpose of utilizing several proxies is to estimate the respective

Ann. Geophys. Discuss., https://doi.org/10.5194/angeo-2019-34
Manuscript under review for journal Ann. Geophys.
Discussion started: 8 March 2019

correlation and the ionospheric delay to identify proxies which are most suitable for describing the solar-ionosphere relationship at different time scales and under different solar activity conditions. Therefore, the ionospheric delay along with the different oscillation periods of solar irradiance are addressed to investigate the GTEC response to solar variations as indicated by various solar proxies. To understand the variability in the ionosphere, we use the method of empirical orthogonal functions (EOF) and classify the temporal and spatial variability in the ionosphere by decompositions into temporal and spatial contributions.

2 Data Sets

Global TEC maps for the period 1999 to 2017 are available from the International GNSS Service (IGS, Hernandez-Pajares et al., 2009). We used NASA's 2-hourly global TEC maps, which are available in IONEX format from the CDDIS (ftp://cddis.gsfc.nasa.gov/gnss/products/ionex/; Noll, 2010) data archive service (CDDIS, 2018). These maps are available in a spatial resolution of 2.5° in latitude and 5° in longitude. We selected 12 solar proxies for the GTEC correlation analysis, namely the F10.7 index (solar radio flux at 10.7 cm, measured in solar flux units (sfu); Tapping, 1987), the Bremen (IUP, 2017) composite Mg-II index (core-to-wing ratio of the Magnesium K line; Maruyama, 2010), Ca K index, DSA (daily sunspot area), He-II (Dudok de Wit, 2011), and F1.8, F3.2, F8, F15, F30 solar radio flux emission at 5 wavelengths (Dudok de Wit et al., 2014, Haberreiter et al., 2017) as well as Ly-α and SSN (sunspot number, Wolf 1856) indices which are available from NASA´s Goddard Space Flight Center through the OMNIWeb Plus database. The F10.7 index data were taken from the LISIRD (DeWolfe et al., 2010) database, whereas F1.8, F3.2, F8, F15, F30, Ca K index and DSA proxies are available from the SOLID database (http://projects.pmodwrc.ch/solid/; Schöll et al., 2016; Haberreiter et al., 2017). SOLID data were only available for the time interval 1999-2012 and all other cover the full period from 1999 till 2017. The daily TEC and GTEC values were calculated from the gridded 2-hourly TEC maps to obtain a time resolution corresponding to those of the solar proxies. Further, to investigate the relation between GTEC and geomagnetic activity, we have used daily Kp, Dst, and Ap indices, which were taken from the OMNIWeb Plus database.

3 Results and discussion

3.1 Long-term variations of TEC and EUV flux

In the following, we analyse the long-term variations in GTEC and EUV flux for the period 1999 till 2017, which partially covers the solar cycles (SC) 23 and 24. The temporal variation of the calculated zonal mean GTEC is shown in Figure 1(a). In SC 23, the TEC values at low latitudes reach up to 80 TECU, while during SC 24 TEC was considerably smaller, which confirms that the zonal mean TEC behaviour is strongly depending on the solar activity. The amount of free electrons in the ionosphere mainly depends on the photoionisation of atomic and molecular neutrals due to solar EUV radiation along with the recombination at different height and solar zenith angle. The lowest TEC values are observed in the year 2008 and 2009 during the extended solar minimum of SC 23. The zonal mean plot additional temporal variations are visible which result from annual and

semi-annual variations in the ionosphere. The spatial distribution of the ionospheric plasma in Fig. 1(a) shows the well-known fountain effect, with maximum TEC values concentrated North and South of the magnetic equator. Figure 1(b) shows the normalised time series of twelve solar proxies for the available data in the analysed time period 1999-2017. As the ionosphere response to solar radiation is varies for different wavelengths, we used twelve solar proxies based on different measurement techniques and spectral characteristics. E.g. Hocke (2008) analysed the GTEC and Mg-II index observations and showed that 1% change in Mg-II index results in about 22% change in GTEC. As all the time series in Figure 1 show a similar overall variation during the 11-year solar cycle, the fundamental behaviour of solar radiation emission is identical at all the wavelengths.

Figure 2 shows the spatial variation of TEC averaged over the period 1999 to 2017 where the superimposed white contour lines show the standard deviation calculated from the daily TEC data. A similar analysis has been shown by Guo et al. (2015) using the same TEC dataset within the period 1999 till 2013, finding a comparable spatial distribution. The maximum TEC values are distributed along the equator around ±20° and decrease towards the poles. Maximum values of the standard deviation are observed in the low latitude region with about 15 TECU. The spatial distribution of TEC depends on the ionisation of neutrals, transport processes, and recombination, which varies with latitude and longitude.

Note that the T-I system is not only influenced by solar activity but also by changing geomagnetic conditions due to solar wind variations. Strong solar activity during solar maxima might induce stronger interaction of the solar wind with earth upper atmosphere, causing ionospheric disturbances at high latitudes along magnetic field lines visible in enhanced TEC values. During solar maxima, the T-I regime can partially be controlled by the solar activity superseding the solar radiation impact. Whereas in periods with low solar activity, the local variability in the ionosphere is also not only regulated by the solar radiation but can be influenced by lower atmospheric forcing (Forbes et al., 2000, Koucká Knížová et al., 2015).

3.2 Spectra of GTEC and solar proxies

The datasets mentioned above are used to understand the oscillatory behaviour of the T-I system. The periodicities in the solar proxies have been studied by various authors to explore the response of the terrestrial atmosphere and especially the T-I region. Here we will investigate and compare the different temporal pattern of GTEC and multiple solar proxies, since proxies may differ in their periodicity depending on the underlying source mechanism.

The cross-wavelet technique from Grinsted et al. (2004) was applied, where Morlet wavelets were used as mother functions. The cross-wavelet technique allows to indicate common high-power regions between two-time series. This allows to determine dominant joint oscillations of the ionosphere and important solar proxies. The cross-wavelets analyses of GTEC with four selected solar proxies are shown in Figure 3. The most dominant periods observed are in the 16-32 days period region visible in all GTEC solar proxy relations during solar maxima. This is, however, not the case during solar minimum when the ionospheric variation due to the

solar activity is lower, and the influence of other dynamical processes in the ionosphere (e.g. lower atmospheric forcing) is stronger. Another high-power region is visible in the 128-256 days period, representing the semi-annual oscillations in both GTEC and solar parameters. The semi-annual oscillation is mostly dominant during the solar maximum years 2001-2002 and 2011-2012. The black arrows in Figure 3 indicate the phase relationship between solar proxies and GTEC. As expected, in the region of 16-32 days GTEC is broadly in phase with the solar proxies, whereas this behaviour is not consistent at the annual and semiannual period range. The most dominant joint annual oscillations are observed between GTEC and Ly-α. Annual oscillation can be found mostly during solar maximum. To summarize, ionospheric TEC variations are strongly connected with the formation of the active regions on the solar surface during the 27 days mean solar rotation period.

To examine the oscillatory behaviour in GTEC and solar proxies more precisely, the Lomb Scargle periodogram LSP (Scargle 1982; Lomb 1976) technique has been used. The corresponding spectral analysis is shown in Figure 4. In this analysis, we have used seven days smoothing windows to get clear spectral features, where the power has been converted into logarithmic scale. In this analysis, data from 1999 till 2012/2017 have been used. The dominant frequencies observed in the GTEC are 27 days, annual, and semi-annual. The observed periodicities in GTEC are also shown by Hocke (2008). Clearly visible in all the solar proxies as well as in GTEC are the mean solar rotation period of about 27 days. It is interesting to note here that a 44-day periodicity is observed in GTEC and all other solar proxies. In the MG-II index, which is widely used to represent the solar variability, the dominant frequencies observed are the 27 days, and it's 2nd harmonic 13.5 days, and 4th harmonic 6.7 days as also described by Hocke (2008). Here a similar kind of oscillations is also visible in the Ly-α spectrum. In the F1.8 index, the annual frequency is observed. A semi-annual oscillation is seen in GTEC. This variation is associated with a dynamical effect of the atmosphere (Liu et al., 2006). Note that the wavelet spectra show some periodicity at the half-year time scale, but with variable phase so that they extinguish in the periodogram.

To evaluate the relation between the solar proxies and GTEC, we analysed the wavelet cross-correlation for the different periods 8-16 days, 16-32 days, 32-64 days, and 64-128 days using the wavelet cross-correlation sequence method using the Maximal Overlap Discrete Wavelet Transform (MODWT) technique (Percival and Walden, 2000). We utilized the MODWT technique, which is a modified version of the discrete wavelet transform from Mallat (1989). In Figure 5 these cross-correlation coefficients are indicated by the background colour, while the inserted numbers show the ionospheric delay in days. The delay is mostly positive or zero, which means that TEC is following the solar proxies with delay. On the 8-16 days time scale, maximum correlation is found for He-II with a correlation coefficient of about 0.62, and second maximum correlation is observed for the F15 index, both with a lag of about one day. The lowest correlation of about 0.25 is found for the F1.8 index. Compared to the 8-16 days period range, the 16-32 days period shows much stronger correlation with more than about 0.6 for all the proxies. Here a maximum correlation of about 0.9 is observed for the He-II and MG-II index, with GTEC delay of about one day. The F30 index and the Ly-α index also show a strong correlation. The lowest correlation of 0.59 is seen for the DSA index. A similar result can be observed in the 32-64 days period range. Here, a maximum correlation is observed again for the He-II and MG-II indices

having a correlation coefficient of 0.9 and a delay of about two days. Another particular strong correlation of about 0.8 is observed with Ly-α and Ca K having a GTEC delay of about one and two days, respectively. Only a weak correlation of about 0.5 with small GTEC lag time is seen for DSA. The similar behaviour in the 16-32, and 32-64 days period ranges is owing to the fact that the solar rotation period of 27 days is only a mean value and different solar regions rotate with a different velocity which can be up to 35 days. This results in strong correlations observable also in the 32-64 days period. In the 64-128 days period range, a longer time lag is reached with above five days for several proxies. Here maximum correlation is found for He-II index with about 0.6 and weakest correlation is seen with about 0.4 for the F1.8 index. Generally, the MG-II and He-II proxies show the strongest correlation with GTEC for all period intervals. A stronger correlation is also seen for Ly-α and F30, while the weakest correlation is seen for F1.8 and DSA

Figure 6 shows the wavelet variance estimated for the GTEC and F10.7 using the MODWT technique with Daubechies 2 (db2) wavelet filter. The wavelet method is widely used to describe the variance of the dataset at different scales. We have selected the time series from the years 2000 to 2002 (maximum of SC 23) and 2012 to 2014 (maximum of SC 24). The red/black colour in the plot represents the SC 23/SC 24 maximum. In GTEC maximum variance appears in the 64-128 days period, which is about a quarterly annual oscillation, and belongs to the seasonal cycle, during SC 23 followed by the observed variance at the 16-32 days period. A general stronger variance can be observed in SC 23 compared to SC 24 for all the periods. In case of the F10.7 index, the maximum variance is visible at the 16-32 days period, which shows here a predominant variance for the solar rotation period. There is no strong semi-annual cycle visible. Here again, the observed variance during SC 23 is stronger compared to SC 24, which might result from strong high activity period.

3.3 Influence of the solar activity on GTEC

This work aims to understand the interaction between solar radiation and the T-I system especially at the time scale of solar rotation. To scrutinize the consequence of different solar activity levels on the T-I system for inter-annual time scales, we evaluate the running cross-correlation analysis between GTEC and solar proxies as shown in Figure 7. Here 365 days running window is used to analyse the time series. The 365 days running mean MG-II index is added to show the overall solar activity. The correlation with all the solar proxies is smallest during the extended low solar activity phase with a correlation coefficient of about less than 0.2 during the solar minimum in 2008-2009. All solar proxies show similar behaviour during low activity conditions, apart from a different mean level. The correlation coefficient is also decreasing during high solar activity years such as 2002 and 2014 but increases during the recovery phase of solar activity. In comparison to all other solar proxies, He-II and MG-II index show stronger correlation with GTEC, while the lowest correlation is given for SSN.

Figure 8 shows the cross-correlation analysis of (a) F10.7 and (b) MG-II with the global, northern hemisphere (NH), southern hemisphere (SH), low (LL, ±30°), middle (ML, ± (30°-60°)) and high (HL, ± (60°-90°)) latitude mean TEC. As in Figure 7, the correlation of F10.7 with TEC is weaker than the one of MG-II and TEC. The

Ann. Geophys. Discuss., https://doi.org/10.5194/angeo-2019-34
Manuscript under review for journal Ann. Geophys.
Discussion started: 8 March 2019

weakest correlation is observed for HL with maximum correlation coefficients of 0.42 (F10.7) and 0.53 (MG-II) and corresponding ionosphere response time of about two and one days, respectively. The maximum correlation is observed for GTEC and LL TEC with correlation coefficients of about 0.7 (F10.7) and 0.82 (MG-II) for a time delay of about two and one days, respectively. NH and SH is comparable with slightly smaller correlations for NH. There is a weaker correlation for ML compared to LL, but the difference is not as large as the one for HL.

Figure 9 shows the cross-correlation analysis between GTEC and solar proxies separately for each year at the timescale of 16-32 days. To calculate the cross-correlation, the data is filtered for different time scales using the MODWT**.** The upper panel of Figure 9 shows the 365 days running mean F10.7. The delay is given as numbers inserted on the colour-coded cross-correlation for the different solar proxies and time periods. As in Figure 7, the overall trend shows that the correlation is weak during solar minimum and strong during high solar activity periods. The time delay is ranging between zero to three days for all solar proxies, but without obvious regularity with respect to the proxies or the time. As in Figure 5, a generally strong correlation is shown for He-II and MG-II, while DSA and F1.8 indices show the weakest correlation. During the years of low solar activity 2007-2010, an especially weak correlation is visible for F3.2, F1.8 and CaK. The maximum F10.7 index is observed during 2001 with about 181 sfu. During the high solar activity years from 1999 to 2003 and from 2012 to 2014 a strong correlation of about 0.85 is observed in MG-II, He-II, F30 (1999-2003, 2012), and Ly-α except for 2001, when the maximum annual mean F10.7 index is observed. During the maximum of SC 23, the cross-correlation between MG-II, He-II, Ly-α, F3.2, F15 and GTEC is about 0.7 with a delay of about 1-2 days. A weak correlation is observed for F1.8 and CaK. During low solar activity (years 2006-2010, 2016) when the average F10.7 index is below 75 sfu, a stronger correlation is observed between He-II and MG-II and GTEC, with a correlation coefficient of more than 0.6. Only weak correlation during low solar activity is observed for F1.8, CaK, F3.2, and DSA. During moderate solar activity years (2004-2005, 2011, 2015), when the average F10.7 index is about 90-120 sfu, MG-II, He-II, F30, and Ly-α shows stronger correlation with GTEC with a delay of about one day. From the above discussion, it is clear that during low solar activity most of the solar proxies show a weak correlation with GTEC.

In comparison to the 16-32 days time scales, we further analyse the cross-correlation and delay at 32-64 days time scales (Figure A.3 in the appendix). Here the He-II and MG-II indices shows stronger correlation during 1999 to 2012/2017, i.e. even during years of low solar activity, with a delay of about 1-3 days. The Ly-α also shows a stronger correlation except for the year 2002. It is interesting to note that during the year 2002 all the proxies show a weaker correlation of about 0.6 except MG-II and Ly-α. Poor correlation is observed between GTEC and F1.8 or DSA during low solar activity years.

In summary, the most suitable proxy to represent the solar activity at the time scale of 16-32 days and 32-64 days during low, moderate, and high solar activity is He-II. The MG-II index, Ly-α, and F30 also show a strong

Ann. Geophys. Discuss., https://doi.org/10.5194/angeo-2019-34
Manuscript under review for journal Ann. Geophys.
Discussion started: 8 March 2019

correlation with GTEC, but there are some differences between solar maximum and minimum. The F1.8 and DSA cannot adequately represent the solar activity at the solar rotation (16-32 days) time scale.

3.4 Spatial distribution of the ionospheric response time

Here we investigate the inter-annual spatial variability of the ionospheric response to solar variations. Figure 10 shows correlation and time lag between TEC and MG-II globally for a TEC map resolution of 2.5° in latitude and 5° in longitude. The left column shows yearly zonal means, while the right column shows 1999 to 2017 means with longitudinal resolution. The contour maps in the upper panel (lower panel) show the cross-correlation (time delay) where the inserted contour lines represent the standard deviation. Maximum correlation of about 0.9 is observed during high solar activity years at low latitudes. Figure 10(a,b) shows that the correlation decreases from low to high latitudes. In the NH, the correlation is the weakest south of the auroral oval, probably due to the fact that particle precipitation also changes with solar wind dynamics. Figure 10(c) shows the zonal mean time delay for the year 1999 to 2017, which is about one day in the low- and mid-latitudes. The delay generally increases towards high latitudes with a few exceptions occurring during low solar activity. There is a tendency that during high solar activity the delay is increased slightly at low latitudes, but strongly (up to 3 days) in the high latitude region. A negative delay is observed during low solar activity, presumably associated with the meteorological effects as suggested by Ren et al. (2018). Another possible reason is ionospheric saturation, which might reduce the transport process during high solar activity due to lower recombination rates. Transport is one of the most critical parameters that control the behaviour of the ionosphere. These results suggest that interannual variability depends not only on solar activity but also on several other physical processes. Lee et al. (2012) analysed electron density measurements from CHAMP and GRACE along with Global Ionosphere Maps (GIM) TEC maps in relations to the F10.7 index and showed the spatial distribution of delay and correlation coefficient during the years 2003 to 2007. They found a strong (weak) correlation between GIM TEC and F10.7 at the mid (high) latitude region, with a time delay of about 1-2 (2-4) day(s) which confirms qualitatively our results. Figure 10(d) shows the spatial distribution of the time delay, where an overall time delay of about one day with a standard deviation of less than one day is visible. The time delay is longer for the high latitude region, whereas the cross-correlation is weaker as can be seen in Figure 10(b). In this region, the standard deviation is more than one day.

3.5 EOF analysis of ionospheric TEC

Ionospheric TEC is varying diurnally, daily, seasonally, on a decadal scale, as well as in latitude and longitude. To examine the spatial variability of TEC, we applied the principal component analysis (PCA) for signal decomposition (Bjornson and Venegas, 1997) using Empirical Orthogonal Function (EOF), which decomposes data into orthogonal modes of variability. This method has been used to represents the variability in the T-I system and for T-I modelling (e.g., Zhao et al., 2005, Matsuo et al., 2012, Ercha et al., 2012, Anderson and Hawkins, 2015, Talaat and Zhu, 2016). We analysed the normalized TEC data sets in a spatial grid of 71×72 (latitude and longitude) and a temporal length of 6940 days. Figure 11 shows the first four EOF maps in the

upper panel followed by the principal components (middle panel) and the corresponding wavelet spectra (lower panel). The first three EOFs are similar to those presented by Talaat and Zhu (2016). The first (second) EOF component explains approximately 86% (11%) of the variance. The first two components capture almost all of the TEC variance, while the third and fourth component only contributes to about 2%. This is similar to results of Zhao et al. (2005), Anderson and Hawkins (2015), and Talaat and Zhu (2016) who reported that more than 95% of the variance is explained by the first three EOFs.

EOF1 shows the spatial distribution of TEC variance in general and is positive everywhere. A high variability in the low latitude region and a smaller one at higher latitudes is shown. This indicates a joint in phase variability of the entire ionosphere, which is larger at low latitudes. Consequently, as is shown in the middle panel of Figure 11, its temporal amplitude varies from positive to negative following the solar activity and the annual cycle. In the lower panel of Figure 11, the wavelet analyses for the EOFs are shown. The wavelet analysis of EOF1 shows a 27 days periodicity associated with the solar rotation period. Annual and semi-annual oscillations are observed especially during the high solar activity years. The EOF2 captures 11% of the total variability and demonstrates the hemispheric asymmetry. The corresponding PC and wavelet analysis show a strong annual variability induced by the eccentricity of the Earth´s orbit in interaction with the annual solar radiation changes in the I-T system. EOF3 captures about 1.79% of the total variability. EOF3 might be associated with non-solar effects or fine structures of the solar activity response which is not captured by the first EOF as suggested by Talaat and Zhu (2016). Note that EOF3 essentially shows a semi-annual and a relatively strong 27-day variability. EOF4 contributes with only 0.4% of the total estimated variability. Its shape is strongly non-zonal and reflects the longitudinal differences of the equatorial ionization anomaly. In the wavelet analysis, only semi-annual and - weaker - annual oscillations are visible.

In order to check the relation between solar proxies and geomagnetic parameters (daily Kp, Dst, and Ap indices) with PCs corresponding to EOFs, cross-correlation and delay is calculated and shown in Figure 12. In Figure 12 the colour indicates the correlation coefficient and the numerical values indicate the corresponding time delay in days. A strong correlation between PC1 and MG-II (F10.7) is observed with a coefficient of about 0.87 (0.8) and a time delay of one (two) day(s). This represents the strong correlation between global TEC and solar variability as PC1 is associated with solar variability. The geomagnetic parameters are generally more loosely connected with ionospheric variability, indicating the relatively fast ionospheric storm reaction compared to the longer lasting equatorial magnetic field depletion. PC3 shows a relatively strong correlation with the geomagnetic parameters, which indicates that this component captures the geomagnetic activity as well as the remaining part of EOF1. Here the Kp and Ap index shows a positive correlation of about 0.6 with the delay of about two days. In comparison to this, a negative correlation of about 0.7 is observed in the Dst.

To assess the variability on the time scale of solar rotation period we have filtered the GTEC time series in a period range of 25 to 35 days using a digital bandpass filter. The filtered time series is then used to compute EOFs. Figure 13 shows the first four EOF components in the upper row, and their corresponding wavelet transforms in the lower row. The first component is capturing almost 85.50 % of total variability, which seems

to be associated with the solar activity. EOF1 shows high variability in the equatorial region. EOF2 captures 8.91 % of variability, and it is partly associated with hemispheric variability. EOF3 captures the variability of 4.92 % which is not captured in the EOF2 component (in particular the hemispheric asymmetry). EOF2 does not show clear hemispheric signal any more, while EOF3 now does. The lower panel shows the corresponding wavelet spectra of PCs. Wavelet analysis shows clearly the expected periodicity in the 16-32 days period in all the PCs, with a response to the 11 years solar cycle.

Furthermore, cross-correlation analysis has been performed to understand the relation between solar proxies and geomagnetic parameters (with PCs corresponding to EOFs of the filtered data as shown in Figure 13) and shown in Figure 14. It shows similar kind of results as in Figure 12 in the case of PC1. PC2 and PC3 are associated with the geomagnetic activities. As compared to Figure 12, PC2 shows good correlation with magnetic indices. So, the distribution of variance is different here. This is because the coupled low-latitude/high-latitude magnetically forced variability, which is mainly represented by PC3 in the case of unfiltered data, is now distributed among PC2 and PC3 for the solar rotation period.

4. Summary

We have investigated the long-term ionospheric response during different solar activity, different timescales and spatial variations using twelve solar proxies (F10.7, F1.8, F3.2, F8, F15, F30, He-II, MG-II index, Ly-α, CaK, DSA, and SSN) and 18 years (1999-2017) of IGS TEC data. The cross-wavelet and LSP methods was used to examine the oscillatory behaviour. The cross-wavelet analysis represents the 16-32 days period in all the solar proxies and GTEC. The maximum correlation with GTEC is observed between the He-II index, MG-II index and F30 in the period range of 16-32 days along with a time delay of about one day. Wavelet variance estimation suggests that GTEC variance is high for the 64-128 days period followed by 16-32 days, while the F10.7 index is showing high variance for the 16-32 days period.

Interannual variation of the cross-correlation analysis suggests that correlation is varying with the solar activity. The most suitable proxy to represent the solar activity at the time scales of 16-32 days and 32-64 days during low, middle and high solar activity is He-II. The MG-II index, Ly-α, and F30 may be placed at the second as these indices show a strong correlation with GTEC, but with some differences between solar maximum and minimum. The F1.8 and DSA poorly represent the solar activity effect on TEC. The spatial distribution of cross-correlation and time was estimated using the MG-II index. The results show significant temporal and spatial variations. Stronger correlation is observed near the equatorial region with a time delay of about 1-2 days. The magnetospheric inputs probably strongly influence both high and low latitude regions, but with a different sign.

TEC datasets also have been decomposed using EOFs along with the principal components analysis method to signify the spatial and temporal variation. The first EOF component captures more the 86% of the variability,

and the first three EOF components explain 99% of the variance. EOF analysis suggests that the 1st component is associated with the solar flux and it varies with latitude and longitude whereas the third component of EOF is strongly associated with the geomagnetic activity.

Data availability. IGS TEC data are provided via NASA through ftp://cddis.gsfc.nasa.gov/gnss/products/ionex/ (CDDIS, 2017). Daily F10.7 index can be downloaded from http://lasp.colorado.edu/lisird/noaa_radio_flux. MG-II index data are provided by IUP at http://www.iup.uni-bremen.de/UVSAT/Datasets/mgii (IUP, 2017). Solar proxies F30, F15, F8, F3.2, F1.8, CaK index, and DSA are available from the SOLID database (http://projects.pmodwrc.ch/solid/). The SSN, Ly-α, Kp, Dst, and Ap indices are provided by NASA´s Goddard Space Flight Center through https://omniweb.gsfc.nasa.gov.

Author contributions. CJ, RV, and JB designed the study. RV analysed the data. RV drafted the first version of the manuscript. All authors discussed the results and provided critical feedback and contributed to the final version of the manuscript.

Competing interests. C. Jacobi is one of the Editors-in-Chief of Annales Geophysicae. The authors declare that they have no conflict of interest.

Acknowledgements. We kindly acknowledge for the provision and NASA for providing of IGS TEC data (NASA) , through ftp://cddis.gsfc.nasa.gov/gnss/products/ionex/ (CDDIS, 2017) and the daily F10.7 index (NOAA), MG-II data (IUP), solar proxies F30, F15, F8, F3.2, F1.8, CaK index, DSA (SOLID database) and SSN, Ly-α, Kp, Dst, and Ap indices (NASA's Goddard Space Flight Center). The study has been supported by Deutsche Forschungsgemeinschaft (DFG) through grants No. JA 836/33-1 and BE 5789/2-1.

References

Afraimovich, E. L., Astafyeva, E. I., Oinats, A. V., Yasukevich, Yu. V., and Zhivetiev, I. V.: Global electron content: a new conception to track solar activity, Ann. Geophys., 26, 335–344, https://doi.org/10.5194/angeo-26-335-2008, 2008.

Anderson, P. C. and Hawkins J. M.: Topside ionospheric response to solar EUV variability, J. Geophys. Res., 121, 1518–1529, https://doi.org/10.1002/2015JA021202, 2016.

BenMoussa, A., Gissot, S., Schühle, U., Del Zanna, G., Auchère, F., Mekaoui, S., Jones, A. R., Walton, D., Eyles, C. J., Thuillier, G., Seaton, D., Dammasch, I. E., Cessateur, G., Meftah, M., Andretta, V., Berghmans, D., Bewsher, D., Bolsée, D., Bradley, L., Brown, D. S., Chamberlin, P. C., Dewitte, S., Didkovsky, L. V., Dominique, M., Eparvier, F. G., Foujols, T., Gillotay, D., Giordanengo, B., Halain, J. P., Hock, R. A., Irbah, A., Jeppesen, C., Judge, D. L., Kretzschmar, M., McMullin, D. R., Nicula, B., Schmutz,W., Ucker, G., Wieman, S., Woodraska, D., and Woods, T. N.: On-orbit degradation of solar instruments, Sol. Phys., 288, 389–434, https://doi.org/10.1007/s11207-013-0290-z, 2013.

Bjornson, H. and Venegas S.A.: A manual for EOF and SVD Analyses of climatic Data, CCGCR Report, 97(1), 112-134, 1997.

CDDIS: GNSS Atmospheric Products, available at: http://cddis.nasa.gov/Data_and_Derived_Products/GNSS/atmospheric_products.html, last access: 15 August 2018.

Chen, Y., Liu, L., and Wan, W.: The discrepancy in solar EUV-proxy correlations on solar cycle and solar rotation timescales and its manifestation in the ionosphere, J. Geophys. Res., 117, A03313, https://doi.org/10.1029/2011JA017224, 2012.

DeWolfe, A. W., Wilson, A., Lindholm, D. M., Pankratz, C. K., Snow, M. A., and Woods, T. N.: Solar Irradiance Data Products at the LASP Interactive Solar Irradiance Data center (LISIRD), In: AGU Fall Meeting 2010, Abstract GC21B-0881, 2010.

Dudok de Wit, T., Bruinsma, S., and Shibasaki, K.: Synoptic radio observations as proxies for upper atmosphere modelling, J. Space Weather Space Clim., 4, A06, https://doi.org/10.1051/swsc/2014003, 2014.

Dudok de Wit, T.: A method for filling gaps in solar irradiance and solar proxy data, A&A, 533, A29, https://doi.org/10.1051/0004-6361/201117024, 2011.

Ercha, A., Zhang, D., Ridley, A. J., Xiao, Z., and Hao, Y.: A global model: Empirical orthogonal function analysis of total electron content 1999–2009 data, J. Geophys. Res., 117, A03328, https://doi.org/10.1029/2011JA017238, 2012.

Forbes, J., Palo, S., and Zhang, X.: Variability of the ionosphere, In J. Atmos. Sol.-Terr. Phys., 62, 685-693, https://doi.org/10.1016/S1364-6826(00)00029-8, 2000.

Grinsted, A., Moore, J. C., and Jevrejeva, S.: Application of the cross wavelet transform and wavelet coherence to geophysical time series, Nonlinear Proc. Geoph., 11(5/6), 561-566, https://doi.org/10.5194/npg-11-561-2004, 2004.

Guo, J., Li, W., Liu, X., Kong, Q., Zhao, C., and Guo, B.: Temporal-spatial variation of global GPS-derived total electron content 1999–2013, PloS one, 10(7), https://doi.org/10.1371/journal.pone.0133378, 2015.

Haberreiter, M., Schöll, M., Dudok de Wit, T., Kretzschmar, M., Misios, S., Tourpali, K., and Schmutz, W.: A new observational solar irradiance composite, J. Geophys. Res., 122, 5910–5930, https://doi.org/10.1002/2016JA023492, 2017.

Hernandez-Pajares, M., Juan, J. M., Sanz, J., Orus, R., Garcia- Rigo, A., Feltens, J., Komjathy, A., Schaer, S. C., and Krankowski, A.: The IGS VTEC maps: a reliable source of ionospheric information since 1998, J. Geodyn., 83, 263–275, https://doi.org/10.1007/s00190-008-0266-1, 2009.

Hocke, K.: Oscillations of global mean TEC, J. Geophys. Res., 113, 1–13, A04302, https://doi.org/10.1029/2007JA012798, 2008.

Jacobi, C., Jakowski, N., Schmidtke, G., and Woods, T. N.: Delayed response of the global total electron content to solar EUV variations, Adv. Radio Sci., 14, 175, https://doi.org/10.5194/ars-14-175-2016, 2016.

Jakowski, N., Fichtelmann, B., and Jungstand, A.: Solar activity control of Ionospheric and thermospheric processes, J. Atmos. Terr. Phys., 53, 1125–1130, https://doi.org/10.1016/0021-9169(91)90061-B, 1991.

Koucká Knížová, P., Z.Mošna, Z., Kouba, D., Potužníková, K., and Boška, J.: Influence of meteorological systems on the ionosphere over Europe, J. Atmos. Sol.-Terr. Phys., 136, Part B, 244-250, https://doi.org/j.jastp.2015.07.017, 2015.

LASP (2018). LASP Interactive Solar Irradiance Data Center, http://lasp.colorado.edu/lisird, last access: 30 July 2018.

Lee, C. K., Han, S. C., Bilitza, D., and Seo, K. W.: Global characteristics of the correlation and time lag between solar and ionospheric parameters in the 27-day period, J. Atmos. Sol-Terr. Phy., 77, 219-224, https://doi.org/10.1016/j.jastp.2012.01.010, 2012.

Liu, L., Wan, W., Ning, B., Pirog, O. M., and Kurvin, V. I.: Solar activity variations of the ionospheric peak electron density, J. Geophys. Res., 111, A08304, https://doi.org/10.1029/2006JA011598, 2006.

Lomb, N.R.: Least-squares frequency analysis of unequally spaced data, Astrophys. Space Sci., 39(2), 447-462, https://doi.org/10.1007/BF00648343, 1976.

Mallat, S.: A theory of multiresolution signal decomposition: The wavelet representation, IEEE Trans. On Pattern Analysis and Machine Intelligence 11,647- 693, 1989.

Maruyama, T.: Solar proxies pertaining to empirical ionospheric total electron content models, J. Geophys. Res., 15, A04306, https://doi.org/10.1029/2009JA014890, 2010.

Matsuo, T., Fedrizzi, M., Fuller-Rowell, T. J., and Codrescu, M. V.: Data assimilation of thermospheric mass density, Space Weather, 10, S05002, https://doi.org/10.1029/2012SW000773, 2012.

Min, K., Park, J., Kim, H., Kim, V., Kil, H., Lee, J., Rentz, S., Lühr, H., and Paxton, L.: The 27-day modulation of the low-latitude ionosphere during a solar maximum, J. Geophys. Res., 114, A04317, https://doi.org/10.1029/2008JA013881, 2009.

Noll, C.: The Crustal Dynamics Data Information System: A resource to support scientific analysis using space geodesy, Adv. Space Res., 45, 1421-1440, https://doi.org/10.1016/j.asr.2010.01.018, 2010.

Percival, D. B. and Walden, A. T.: Wavelet Methods for Time Series Analysis. Cambridge, U.K: Cambridge University Press, 2000.

Ren, D., Lei, J., Wang, W., Burns, A., Luan, X., and Dou, X.: Does the peak response of the ionospheric F2 region plasma lag the peak of 27-day solar flux variation by multiple days? J. Geophys. Res., 123. https://doi.org/10.1029/2018JA025835, 2018.

Scargle, J. D.: Studies in astronomical time series analysis. II-Statistical aspects of spectral analysis of unevenly spaced data, Astrophys. J., 263, 835-853, https://doi.org/10.1086/160554, 1982.

Schmidtke, G., Avakyan, S.V., Berdermann, J., Bothmer, V., Cessateur, G., Ciraolo, L., Didkovsky, L.,Dudoc de Wit, T. ,Eparvier, F.G., Gottwald, A.,Haberreiter, M., Hammer, R., Jacobi, Ch., Jakowski, N., Kretzschmar, M.,Lilensten, J., Pfeifer, M., Radicella, S.M., Schäfer, R., Schmidt, W., Solomon, S.C., Thuillier, G., Tobiska, W. K., Wieman, S., and Woods, T.N.: Where does the Thermospheric Ionospheric GEospheric Research (TIGER) Program go? Adv. Space Res., 56, 1547-1577, https://doi.org/10.1016/j.asr.2015.07.043, 2015.

Schmidtke, G., Nikutowski, B., Jacobi, Ch., Brunner, R., Erhardt, Ch., Knecht, S., Scherle, J., and Schlagenhauf J.: Solar EUV irradiance measurements by the Auto-Calibrating EUV Spectrometers (SolACES) aboard the International Space Station (ISS), Solar Phys., 289, 1863-1883, https://doi.org/10.1007/s11207-013-0430-5, 2014.

Schmölter, E., Berdermann, J., Jakowski, N., Jacobi, C., and Vaishnav, R.: Delayed response of the ionosphere to solar EUV variability, Adv. Radio Sci., 16, 149-155, https://doi.org/10.5194/ars-16-157-2018, 2018.

Schöll M., Dudok de Wit, T., Kretzschmar, M., and Haberreiter, M.: Making of a solar spectral irradiance dataset I: observations, uncertainties, and methods. J. Space Weather Space Clim., 6, A14, https://doi.org/10.1051/swsc/2016007, 2016.

Talaat, E. R. and Zhu, X.: Spatial and temporal variation of total electron content as revealed by principal component analysis, Ann. Geophys., 34(12), 1109-1117, https://doi.org/10.5194/angeo-34-1109-2016, 2016.

Tapping, K. F.: Recent solar radio astronomy at centimeter wave- lengths: The temporal variability of the 10.7 cm flux, J. Geophys. Res., 92, 829–838, https://doi.org/10.1029/JD092iD01p00829, 1987.

Unglaub, C., Jacobi, Ch., Schmidtke, G., Nikutowski, B., and Brunner, R.: EUV-TEC proxy to describe ionospheric variability using satellite-borne solar EUV measurements: first results, Adv. Space Res., 47, 1578-1584, https://doi.org/10.1016/j.asr.2010.12.014, 2011.

Vaishnav, R., Jacobi, Ch., Berdermann, J., Schmölter, E., and Codrescu, M.: Ionospheric response to solar EUV variations: Preliminary results, Adv. Radio Sci., 16, 157-165, https://doi.org/10.5194/ars-16-149-2018, 2018a.

Vaishnav, R., Jacobi, C., Berdermann, J., Schmölter, E., and Codrescu, M.: Ionospheric response during low and high solar activity, Rep. Inst. Meteorol. Univ. Leipzig 56, 1-10, ISBN: 978-3-9814401-6-4, http://meteo.physgeo.uni-leipzig.de/de/orga/LIM_Bd_56.pdf, 2018b.

Wolf, R.: Mittheilungen über die Sonnenflecken, Vierteljahresschrift der Naturforschenden Gesellschaft in Zürich, 1, 151-161, 1856.

Woods, T. N., Bailey, S., Eparvier, F., Lawrence, G., Lean, J., McClintock, B., Roble, R., Rottmann, G. J., Solomon, S. C., Tobiska, W. K., and White, O. R.: TIMED Solar EUV Experiment, Phys. Chem. Earth Pt. C, 25, 393–396, https://doi.org/10.1016/S1464-1917(00)00040-4, 2000.

Zhao, B., Wan, W., Liu, L., Yue, X., and Venkatraman S.: Statistical characteristics of the total ion density in the topside ionosphere during the period 1996–2004 using empirical orthogonal function (EOF) analysis, Ann. Geophys., 23, 3615–3631, https://hal.archives-ouvertes.fr/hal-00318090,2005.

Ann. Geophys. Discuss., https://doi.org/10.5194/angeo-2019-34
Manuscript under review for journal Ann. Geophys.
Discussion started: 8 March 2019

Figures

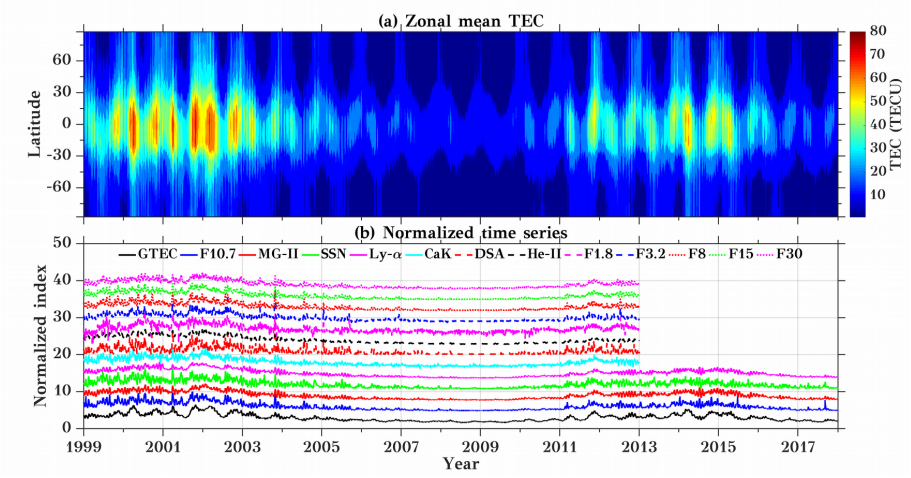

Figure 1: Time series of (a) zonal mean TEC and (b) smoothed normalised datasets of GTEC and different solar proxies for the years 1999 to 2017. The curves in (b) are vertically offset by 3 each. X-axis labels refer to January 1st of the respective year.

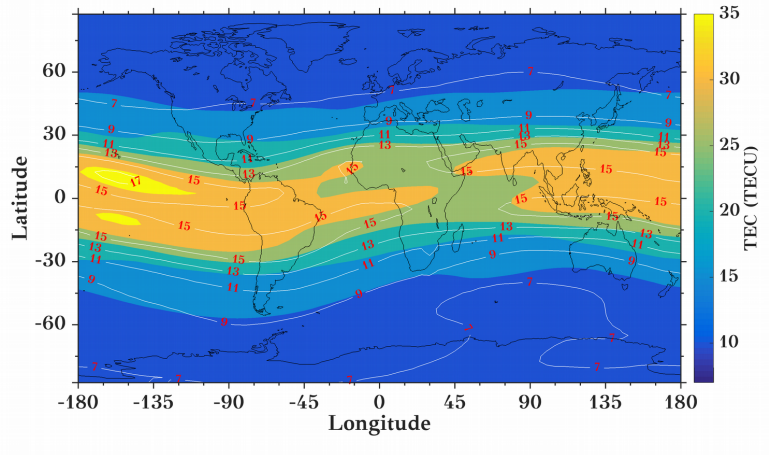

Figure 2: Long-term diurnal and annual mean TEC distribution during the years 1999 to 2017. The white contour lines indicate the standard deviation based on daily data.

Ann. Geophys. Discuss., https://doi.org/10.5194/angeo-2019-34
Manuscript under review for journal Ann. Geophys.
Discussion started: 8 March 2019

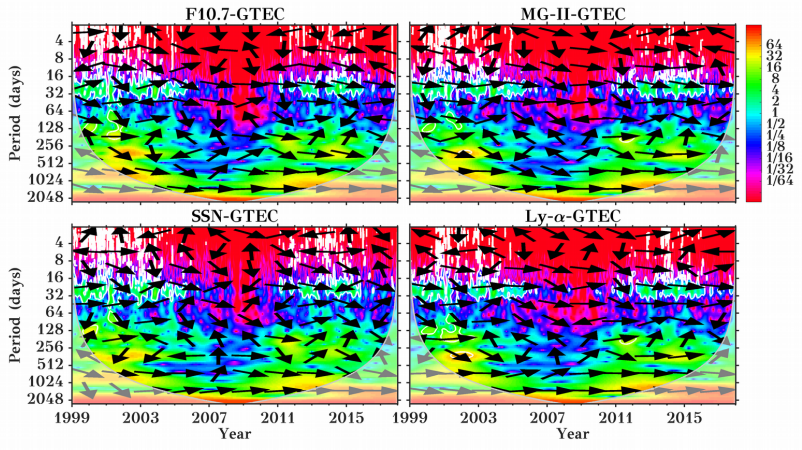

Figure 3: Cross-wavelet spectra for GTEC and different solar proxies during the years 1999 to 2017. The thin gray line shows the cone of influence, where a white line surrounds significant values. The arrows indicate the phase relationship, with in-phase/anti-phase relation shown by arrows pointing to the right/left, while downward direction means that GTEC is leading. X-axis labels refer to January 1st of the respective year.

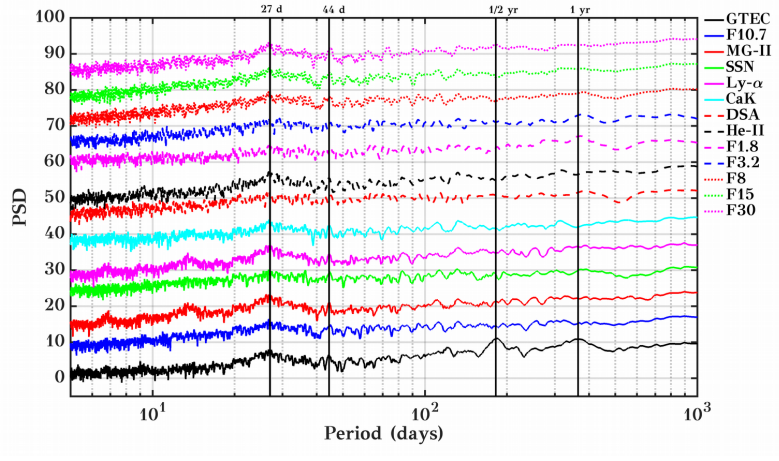

Figure 4: Lomb Scargle periodogram for GTEC and multiple solar proxies. The curves are vertically offset by a factor of 7 each.

Ann. Geophys. Discuss., https://doi.org/10.5194/angeo-2019-34
Manuscript under review for journal Ann. Geophys.
Discussion started: 8 March 2019

Annales Geophysicae Discussions
Open Access
EGU

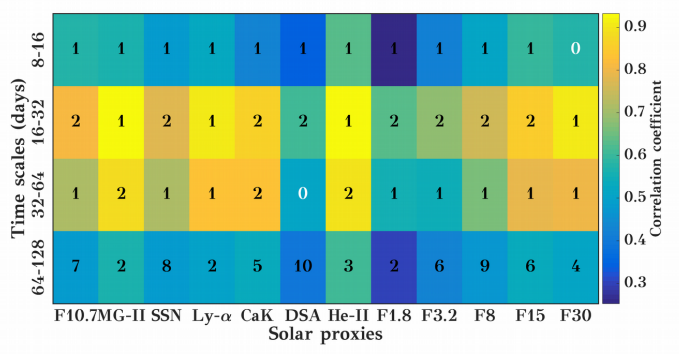

Figure 5: Wavelet cross-correlation sequence estimates for the maximal overlap discrete wavelet transform for GTEC and multiple solar proxies for different time scales (8-16, 16-32, 32-64, and 64-128 days). Background colour shows the correlation coefficient, and the inserted number shows the delay in days.

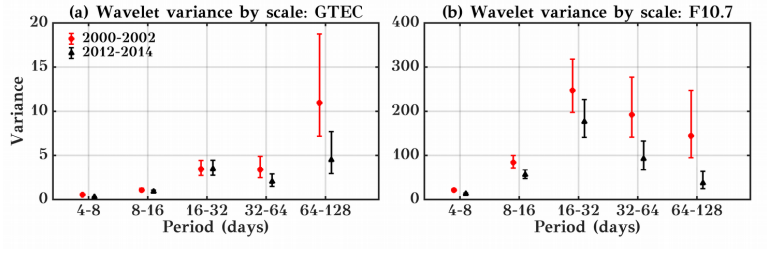

Figure 6: Wavelet variance for the maximums of SC 23 (2000-2002, red) and 24 (2012-2014, black) for (a) GTEC and (b) F10.7. Error bars show the 95% coverage probability of the confidence interval obtained from the 'Chi2Eta3' confidence method.

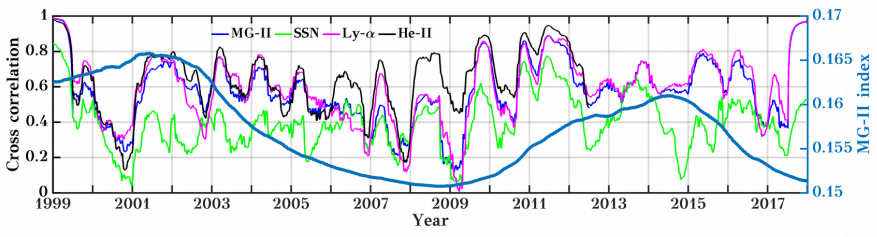

Figure 7: Running cross-correlation between GTEC and different solar proxies. A 365 days running window is used to calculate the correlation. The second y-axis shows 365 days running mean time series of MG-II index.

Ann. Geophys. Discuss., https://doi.org/10.5194/angeo-2019-34
Manuscript under review for journal Ann. Geophys.
Discussion started: 8 March 2019

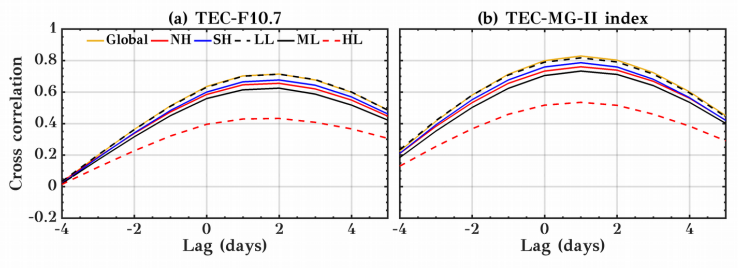

Figure 8: Cross-correlation coefficients and time delays between the Global, northern hemisphere (NH), southern hemisphere (SH) as well as low (LL, ±30°), middle (ML, ± (30°-60°)) and high (HL, ± (60°-90°)) latitude TEC with (a) F10.7 and (b) MG-II index during the years 1999 to 2017. A positive lag means that solar flux variations are heading TEC ones.

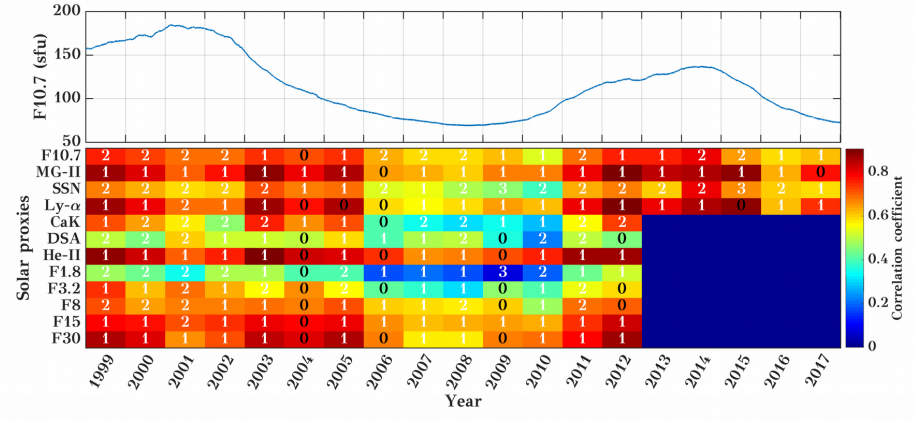

Figure 9: In the upper panel 365 days running mean time series of F10.7 is shown. The lower panel displays yearly cross-correlations and time delays between GTEC and different solar proxies for the years 1999 to 2017 at the timescale of 16-32 days. The background colours show the correlation coefficient and the inserted numbers show the delay in days.

Ann. Geophys. Discuss., https://doi.org/10.5194/angeo-2019-34
Manuscript under review for journal Ann. Geophys.
Discussion started: 8 March 2019

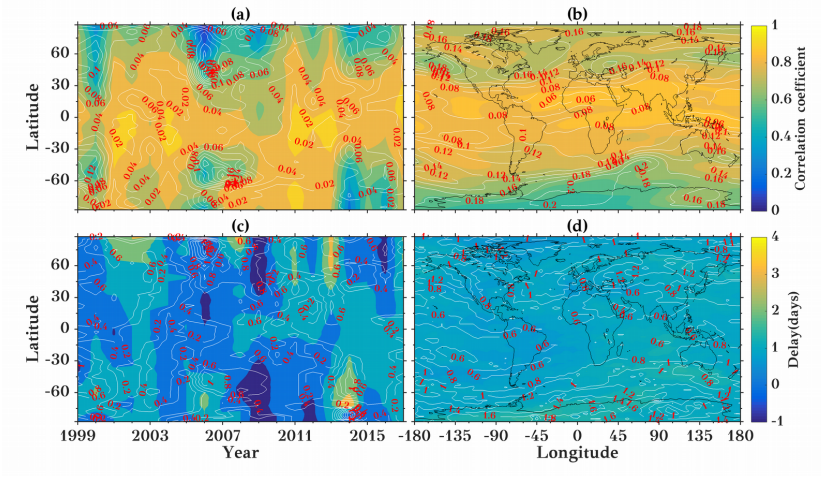

Figure 10: (a,c) zonal mean and (b,d) long-term mean correlation coefficients (upper row) and time delay (lower row) between TEC and MG-II index for the years 1999 to 2017. The white contour lines indicate the respective standard deviations.

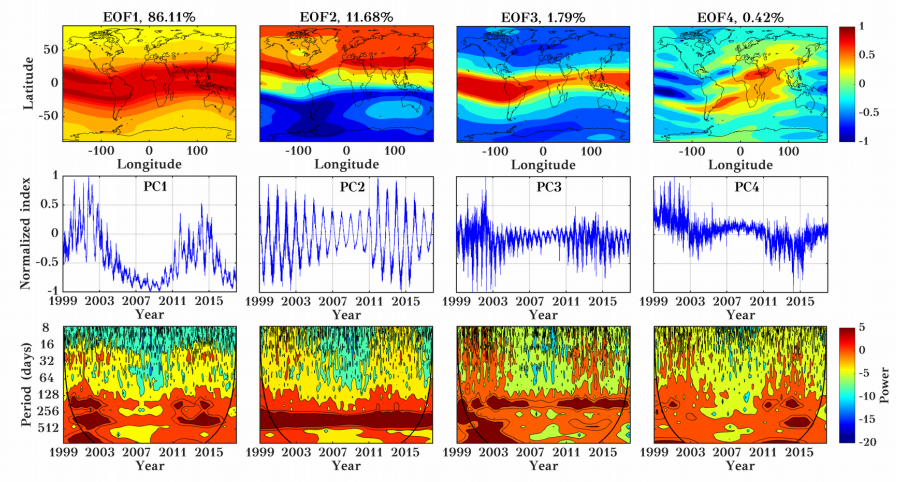

Figure 11: The first four EOFs (top row) of normalized TEC during the years 1999 to 2017, corresponding principal components (middle row), and their corresponding wavelet transform (bottom row). Please note that EOFs are dimensionless.

20

Ann. Geophys. Discuss., https://doi.org/10.5194/angeo-2019-34
Manuscript under review for journal Ann. Geophys.
Discussion started: 8 March 2019

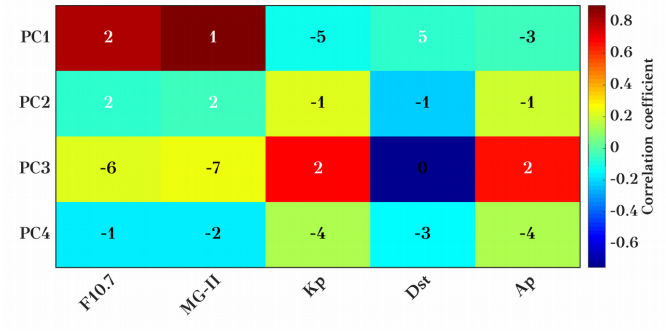

Figure 12: Correlation coefficients and time lag between the PCs and solar and geomagnetic proxies.

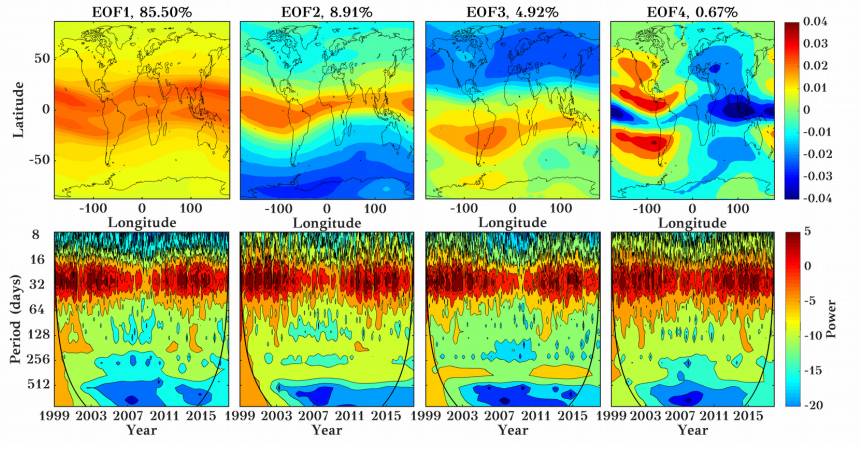

Figure 13: Spatial distribution map of first four EOFs (top row) of IGSTEC during the year 1999 to 2017, and their corresponding wavelet transform (bottom row) using a 25-35 days filtered datasets. The EOFs are dimensionless.

Ann. Geophys. Discuss., https://doi.org/10.5194/angeo-2019-34
Manuscript under review for journal Ann. Geophys.
Discussion started: 8 March 2019

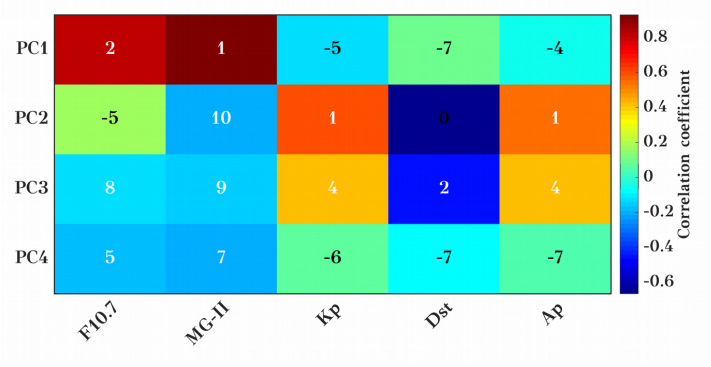

Figure 14: Correlation coefficients and time lag between the PCs and solar and magnetic proxies for the 25-35 days period range.

Ann. Geophys. Discuss., https://doi.org/10.5194/angeo-2019-34
Manuscript under review for journal Ann. Geophys.
Discussion started: 8 March 2019

Annales Geophysicae Discussions
Open Access
EGU

Appendix A: Figures

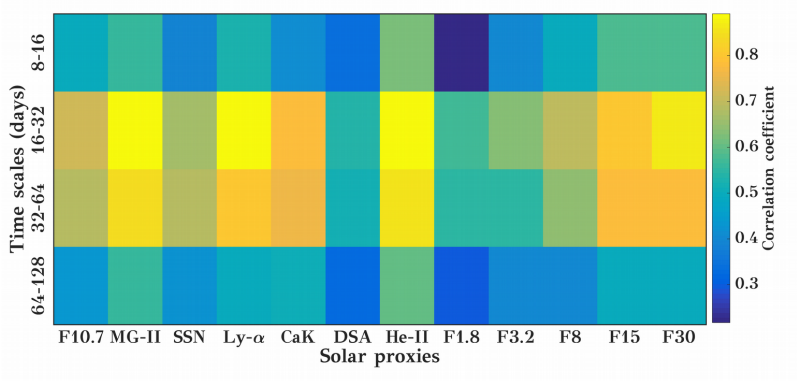

A.1: Wavelet cross-correlation sequence estimates for the maximal overlap discrete wavelet transform for GTEC and multiple solar proxies for different time scales (8-16, 16-32, 32-64, and 64-128 days). Background colour shows the correlation coefficient at lag 0.

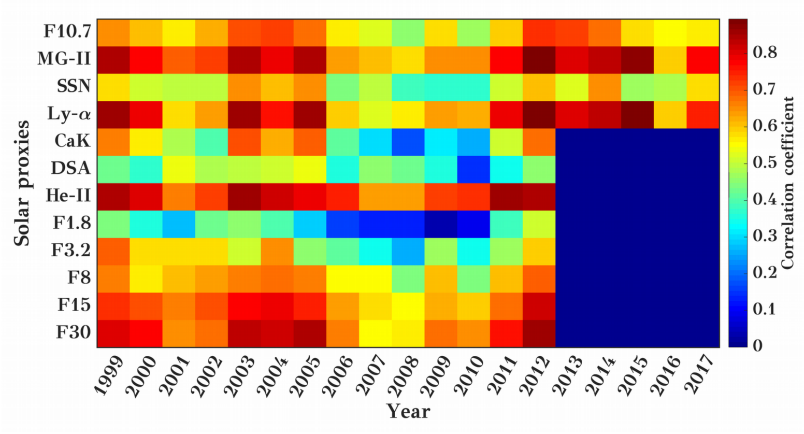

A.2: Cross-correlation between GTEC and different solar proxies for years 1999 to 2017 at the timescale of 16-32 days at lag 0. Background colours show the correlation coefficients.

Ann. Geophys. Discuss., https://doi.org/10.5194/angeo-2019-34
Manuscript under review for journal Ann. Geophys.
Discussion started: 8 March 2019

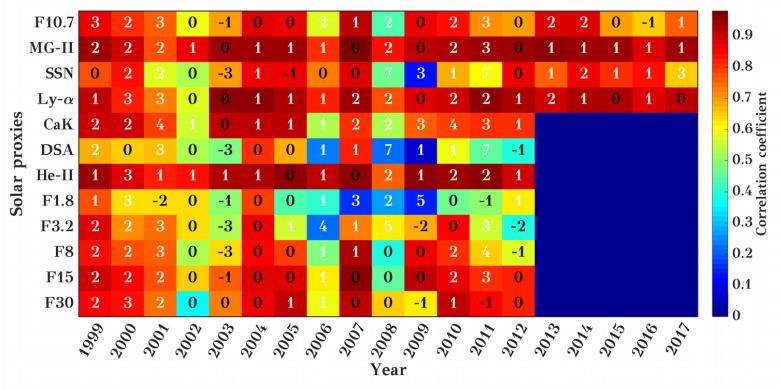

A.3: Cross-correlation and time delay between GTEC and different solar proxies for the years 1999 to 2017 at the timescale of 32-64 days. Background colours show the correlation coefficients, and the inserted numbers show the delay in days.

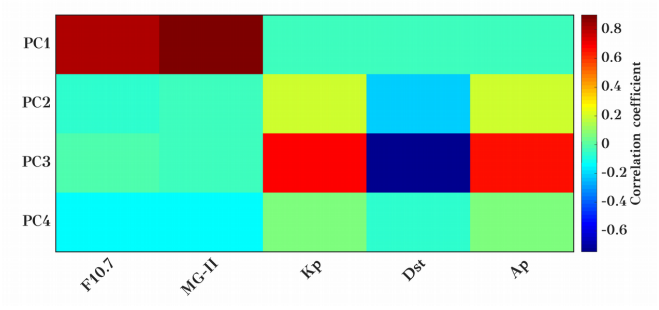

A.4: Correlation coefficients between the PCs and solar/geomagnetic proxies at lag 0.

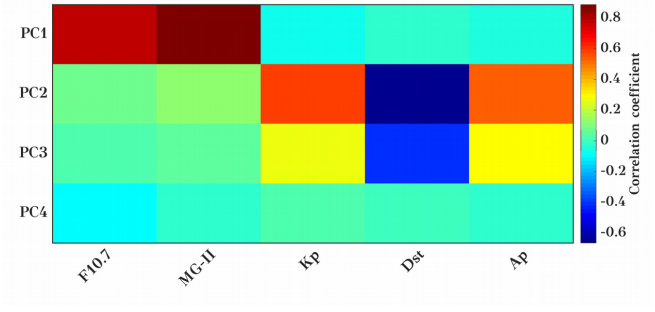

A.5: Correlation coefficients between the PCs and solar and magnetic proxies for the 25-35 days period range for zero lag.